

Article

Inerter Location-Based Vibration Suppression Study of a Transmission Line Equipped with Tuned-Mass-Damper-Inerter (TMDI) under Harmonic Excitation

Xinpeng Liu ^{1,2} , Yingwen Yang ^{1,2,*}, Yi Sun ^{1,2} , Yongli Zhong ^{1,2,*}  and Lei Zhou ^{1,2}

¹ School of Civil Engineering and Architecture, Chongqing University of Science & Technology, Chongqing 401331, China; liu_simple@cqust.edu.cn (X.L.); sunyi@cqust.edu.cn (Y.S.); zlhyy1998@163.com (L.Z.)

² Chongqing Key Laboratory of Energy Engineering Mechanics & Disaster Prevention and Mitigation, Chongqing 401331, China

* Correspondence: yangyingwen2021@163.com (Y.Y.); zhongyongli@cqu.edu.cn (Y.Z.)

Abstract: This paper proposes a novel ungrounded TMDI to improve the vibration suppression performance of the transmission line under harmonic excitation. This type of inerter-based damper may transform a translational motion into a rotational motion, greatly increasing the efficiency of vibration suppression. In the present study, the differential equations of motion are first derived based on the transmission line with an ungrounded TMDI structure. Then the closed-form solution of the displacement response spectrum considering the influence of the suspension location of the inerter is developed. The impact of the inerter location on vibration suppression performance is investigated in depth by defining the suspension location factor (v) and tuning the damping ratio and frequency ratio. The results demonstrate that the suspension location of the inerter has a substantial impact on the damping ratio, frequency ratio, and vibration suppression performance. When the connection location of the inerter is near to the mass of the damper, it degrades the vibration suppression performance of the system. The failure phenomenon of the inerter occurs in the range of $0.2 < v < 0.3$, indicating that the presence of the inerter in this range does not enhance vibration suppression performance. The modal coordinate difference has a considerable impact on the vibration suppression efficacy of the TMDI. With increasing modal coordinate differences, the vibration suppression performance of the TMDI grows dramatically.

Keywords: tuned-mass-damper-inerter (TMDI); transmission line; parameter optimization; vibration control performance



Citation: Liu, X.; Yang, Y.; Sun, Y.; Zhong, Y.; Zhou, L. Inerter Location-Based Vibration Suppression Study of a Transmission Line Equipped with Tuned-Mass-Damper-Inerter (TMDI) under Harmonic Excitation. *Buildings* **2022**, *12*, 657. <https://doi.org/10.3390/buildings12050657>

Academic Editor: Theodore Stathopoulos

Received: 26 April 2022

Accepted: 11 May 2022

Published: 16 May 2022

Publisher's Note: MDPI stays neutral with regard to jurisdictional claims in published maps and institutional affiliations.



Copyright: © 2022 by the authors. Licensee MDPI, Basel, Switzerland. This article is an open access article distributed under the terms and conditions of the Creative Commons Attribution (CC BY) license (<https://creativecommons.org/licenses/by/4.0/>).

1. Introduction

Transmission lines are cable structures made of steel-core aluminum-stranded wire. These kinds of structures subjected to harmonic excitations are prone to vibration due to their light mass and low inherent damping, which will lead to accidents such as wire breakage and phase flashover. Therefore, the vibration suppression of conductors has always been a hot topic of research in the field of civil engineering [1–9]. For the transmission lines, the main source of external excitation is wind force [10,11]. As the most common wind-induced vibration, the vortex-induced vibration (VIV) is excited as periodically shed vortices exert unsteady loads on the surface of the bluff body. Hence, the VIV of transmission lines is a quasi-harmonic vibration, which will cause continuous high-frequency vibration of transmission lines. The tuned mass damper (TMD), a passive vibration control method, has been widely used in vibration control of different kinds of structures [12–17], e.g., marine risers, bridges, pipelines, and heat exchanger tubes. In 1928, a kind of TMD, dubbed the Stockbridge type damper, was proposed by Stockbridge [18], as shown in Figure 1. To date, this kind of dynamic vibration absorber is still employed to mitigate the vibration of transmission lines.

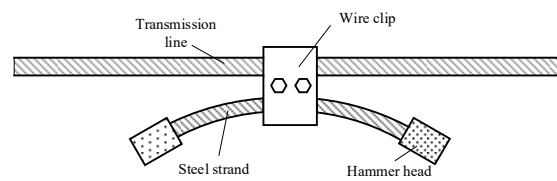


Figure 1. Schematic drawing of a Stockbridge damper.

The damping mechanism of the Stockbridge damper is that the vibration of the cable is transferred to the hammerhead and steel strand by the wire clip. During the vibration process, the sliding friction occurs inside the steel strand, which dissipates the energy and reduces the vibration. By tuning the mass of the hammerhead and the stiffness of the steel strand, the energy dissipation efficiency of the Stockbridge damper can be optimized, thus reducing the structural vibration.

In the past few decades, research on Stockbridge dampers can be divided into two types. One is the research on the vibration features of the Stockbridge damper [19–23]. The other is the performance evaluation of structures [24–26]. Although the Stockbridge damper has the advantages of mechanical simplicity, cost-effectiveness, and excellent vibration suppression performance, there is still a limitation in terms of the effectiveness of vibration control. That is, the vibration control performance of the Stockbridge damper depends on the mass of the hammerhead. However, it is not appropriate to increase the mass of the damper for improving the vibration suppression performance of the structure. Because it will challenge the safety performance of the cable structure.

In 2002, the concept of the inerter element was proposed by Smith [27]. Since then, the research on inerter-based dampers has received a lot of attention. Although the inerter was initially employed in the field of electrical engineering, the corresponding mechanical components with the same property can also be obtained in the field of civil engineering, such as ball screw assembly, rack-and-pinion, hydraulic and viscous type inertial containers, etc. The ideal reaction force of the two terminals is proportional to the relative acceleration of the two terminals, which is expressed as

$$F = b(\ddot{u}_1 - \ddot{u}_2) \quad (1)$$

where \ddot{u}_1, \ddot{u}_2 represent the accelerations at two terminals, and b is the apparent mass factor. By connecting the TMD to the foundation with an inerter, a novel type of damper named the tuned mass damper inerter (TMDI) was proposed by Marian and Giaralis [28], as shown in Figure 2a,b.

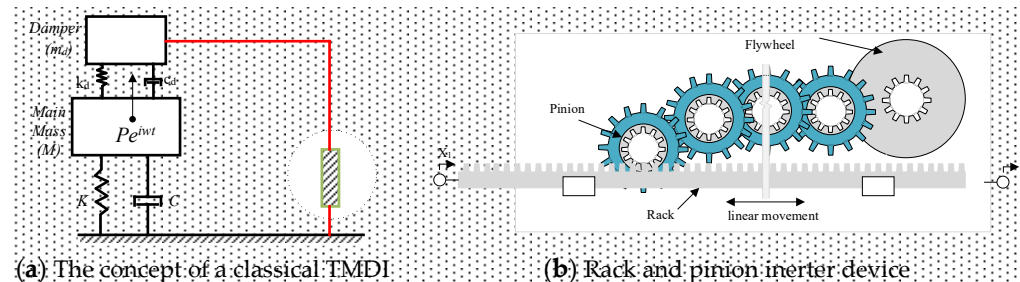


Figure 2. Schematic drawing of TMDI.

Marian and Giaralis [28] indicated that the TMDI is capable of improving the vibration suppression performance of the primary structure while reducing the mass of the damper. Pan and Zhang [29] derived the closed-form stochastic responses of SDOF structures with inerter-based dampers under white-noise loads. By the stochastic vibration response mitigation ratio, empirical expression formulae of the key parameters for the inerter systems were obtained. Giaralis and Petrini [30] indicated that TMDIs are capable of reducing the peak top-floor acceleration more effectively than the TMD. And the incorporation of the

inerters can significantly reduce the energy consumption space of the TMD. Petrini et al. [31] proposed a novel TMDI used to address the occupant comfort issues in wind-induced tall buildings. In addition, the possibility of converting wind vibration energy into electrical energy by TMDIs was discussed. Wang et al. [32] studied the suppression performance of the inerter-based vibration absorbers used in high-rise buildings. Through the wind tunnel tests, the performance-based optimization of the inerter-based vibration absorbers was carried out to balance the vibration mitigation criteria between the displacement and the acceleration of the tall building. Su et al. [33] derived the closed-form solutions for the mitigation performance of TMDI based on a filter approach. Moreover, the quantitative evaluation criterion for the control performance of TMDI was proposed, which indicated that the inerter was capable of enhancing the vibration control performance of the tall buildings subjected to wind and seismic loads. Dai et al. [34] discussed the impact of inerter location on the control performance of flexible structures with TMDIs. The results showed that when the two terminals of the inerter span longer beam length, the TMDI has better control performance. Zhang and Fitzgerald [35] proposed the application of a TMDI for the suppression of the edgewise blade vibration in wind turbines, which showed that the TMDI can maintain high vibration suppression efficiency while reducing the damper stroke up to 55% because of the inclusion of the inerter. In seismic base isolation, De Domenico and Ricciardi [36] proposed to attach the TMDI to the isolation floor for the displacement reduction of structures subjected to seismic activity. Based on the stochastic vibration theory, Domenico derived the expression formulation of the optimal parameters of the TMDI. The results showed that the base-isolation system equipped with optimal TMDI has a high level of control efficiency of both the displacement and the shear of the isolated superstructure.

In addition, the research on the optimization of inerter-based dampers can be divided into two branches. One is the mathematical method, which obtains the analytic solution of the objective function by mathematical derivation. Zhou evaluated the vibration control performance of the DTMDI by the fixed-point theory [37]. Wang and Giaralis [38] studied the effect of the stiffness and mass terms on the vibration suppression performance of the TMDI through a series of experiments on tapered cantilever beams. The other branch involves meta-heuristic algorithms, such as the colliding bodies optimization (CBO) method [39]. Kaveh et al. [40] verified the performance as well as the robustness of high-rise buildings with TMDI through the CBO method.

Compared to the TMD, TMDI not only has a good vibration suppression performance but also has a high potential to reduce the mass of the damper. Hence, this kind of damper has been widely used in vibration control of high-rise buildings, bridge structures, and wind turbines. So far, however, there has been little discussion about the instrument of inerter-based dampers in vibration suppression of transmission lines. The transmission line structure is a cable structure with internal axial tension, which is fundamentally different from traditional high-rise structures, bridge structures, or wind turbine blade structures. The internal tension has a significant effect on the dynamic characteristics of the conductor, so the impact of which cannot be ignored in vibration suppression studies. Furthermore, we prefer to improve the vibration reduction efficiency of dampers per unit mass. As known from the previous studies, the TMDI can simulate a large inertial mass while neglecting its physical mass. Hence, this paper innovatively proposes the utilization of the TMDI in transmission line systems to address the issue that the vibration suppression performance is overly dependent on the mass of the damper. According to the previous research, the grounded TMDI has better vibration suppression performance than TMD. This conclusion theoretically supports the utilization of TMDI for the vibration control of the transmission line. But considering the large height of the transmission line from the ground, the practical application of the grounded TMDI is more difficult. Therefore, the purpose of the present work is to discuss the impact of the inerter connection position on the vibration reduction performance for the ungrounded TMDI and to attempt to propose an ungrounded TMDI that can be used for the vibration suppression of conductors.

The remainder of this paper is organized as follows: the closed-form solution of the displacement response spectrum of the transmission line with an ungrounded TMDI is derived in Section 2. Through parameter optimization, the vibration suppression performance of the system is discussed in detail (Section 3). Finally, the conclusions are summarized in Section 4.

2. Dynamics Model

In this section, a transmission line equipped with an ungrounded TMDI is proposed. The excitation is simulated simplistically as a harmonic force. The schematic diagram of the model is shown in Figure 3.

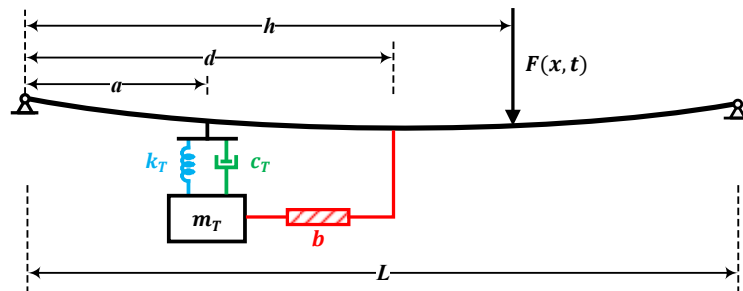


Figure 3. A schematic diagram of a transmission line with TMDI.

2.1. Differential Equations of Motion

Based on the dynamics model, the force analysis is conducted on the micro-segment of the transmission line-ungrounded TMDI system, as shown in Figure 4. The closed-form solution of the displacement response spectrum is derived.

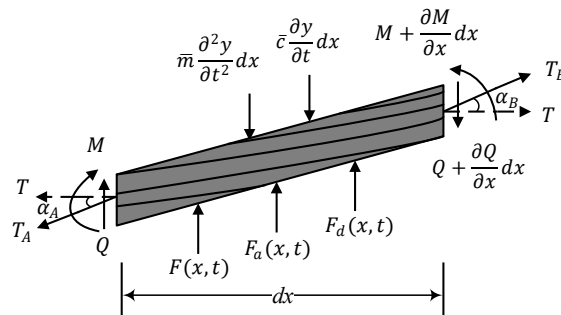


Figure 4. The transmission line element diagram.

In terms of the horizontal balance conditions, the equations can be expressed by

$$T_B \cos \alpha_B - T_A \cos \alpha_A = 0 \tag{2a}$$

where T_A and T_B are the internal tension of the transmission line, which can be decomposed as follows

$$T_A = \frac{T}{\cos \alpha_A} \tag{2b}$$

$$T_B = \frac{T}{\cos \alpha_B}. \tag{2c}$$

According to the vertical direction balance condition, the equation can be given by the following:

$$\begin{aligned} T_B \sin \alpha_B - T_A \sin \alpha_A - \bar{m}(x) \frac{\partial^2 y(x, t)}{\partial t^2} dx - \bar{c}(x) \frac{\partial y(x, t)}{\partial t} dx - \frac{\partial Q}{\partial x} dx \\ = -F(x, t) - F_a(x, t) - F_d(x, t) \end{aligned} \tag{3}$$

in which $\bar{m}(x), \bar{c}(x)$ are the mass and damping of the conductor per unit length along the span direction respectively. $y(x, t)$ is the vertical displacement of the transmission line. $F(x, t)$ is the harmonics force acts on the transmission line. $F_a(x, t), F_d(x, t)$ are the feedback forces from the mass and inerter of the TMDI on the transmission line, respectively.

Based on the balance condition of the bending moment, the equation is obtained by

$$\left(M + \frac{\partial M}{\partial x} dx \right) - M - \left(Q + \frac{\partial Q}{\partial x} dx \right) dx - \bar{m}(x) \frac{\partial^2 y(x, t)}{\partial t^2} dx \frac{dx}{2} + T_B \sin \alpha_B dx - T_B \cos \alpha_B \frac{\partial y(x, t)}{\partial x} dx = 0 \tag{4a}$$

where M and Q are the bending moments and shear force of the cross-section, which are

$$M = EI \frac{\partial^2 y(x, t)}{\partial x^2} \tag{4b}$$

$$Q = \frac{\partial M}{\partial x} = EI \frac{\partial^3 y(x, t)}{\partial x^3} \tag{4c}$$

According to the geometric differential relation of the micro-segment, $\tan \alpha_A$ and $\tan \alpha_B$ are expressed as follows

$$\tan \alpha_A = \frac{\partial y(x, t)}{\partial x} \tag{4d}$$

$$\tan \alpha_B = \frac{\partial y(x, t)}{\partial x} + \frac{\partial^2 y(x, t)}{\partial x^2} dx \tag{4e}$$

Simultaneous with Equations (2)–(4), the differential equation of motion is as follows

$$\bar{m}(x) \frac{\partial^2 y(x, t)}{\partial t^2} + \bar{c}(x) \frac{\partial y(x, t)}{\partial t} + EI \frac{\partial^4 y(x, t)}{\partial x^4} - T \frac{\partial^2 y(x, t)}{\partial x^2} = F(x, t) + F_a(x, t) + F_d(x, t) \tag{5}$$

The harmonics excitation can be expressed as

$$F(x, t) = \delta(x - h) \hat{f}(x) \sin(\bar{\omega}t) \tag{6}$$

where $\hat{f}(x)$ denotes the amplitude of the external force, $\bar{\omega}$ represents the frequency of the harmonic excitation, and δ is the Dirac function, which is

$$\delta(x) = \begin{cases} \infty & x = 0 \\ 0 & x \neq 0 \end{cases} \tag{7}$$

To calculate the feedback forces of $F_a(x, t)$ and $F_d(x, t)$, the dynamic equation for the TMDI is developed as follows:

$$m_T \ddot{y}_T + c_T (\dot{y}_T - \dot{y}_a) + k_T (y_T - y_a) + b (\ddot{y}_T - \ddot{y}_d) = 0 \tag{8}$$

where m_T, k_T, c_T are the mass, stiffness, and damping of the TMDI. y_T is the vertical displacement of the mass of the TMDI. y_a, y_d are the vertical displacements of the transmission line at the suspension location of the mass and the inerter of the TMDI, respectively. $F_a(x, t)$ and $F_d(x, t)$ can be calculated as follows

$$F_a(x, t) = \delta(x - a) [c_T (\dot{y}_T - \dot{y}_a) + k_T (y_T - y_a)] \tag{9}$$

$$F_d(x, t) = \delta(x - d) b (\ddot{y}_T - \ddot{y}_d) \tag{10}$$

The vertical displacement of the line, $y(x, t)$, can be expressed as a linear combination of the vibration modes

$$y(x, t) = \sum_{n=1}^{\infty} u_n(t) \phi_n(x) \quad (11)$$

in which ϕ_n is the n th vibrational modal of the transmission line, which can be expressed as $\phi_n(x) = \sin(n\pi x/L)$; $u_n(t)$ denotes the n th order generalized displacement of the transmission line.

When the n th modal resonance occurs, substituting Equation (11) into Equation (7) and simultaneous Equation (10), ignoring the other modal response [1,35]. The equations of motion of the system can be expressed in matrix form as follows:

$$M\ddot{Y} + C\dot{Y} + KY = F \quad (12)$$

$$M = \begin{bmatrix} M_n - \phi_n(a)\phi_n(d)b + \phi_n^2(d)b & \phi_n(a)(m_T + b) - \phi_n(d)b \\ -\phi_n(d)b & m_T + b \end{bmatrix} \quad (13a)$$

$$C = \begin{bmatrix} C_n & 0 \\ -\phi_n(a)c_T & c_T \end{bmatrix} \quad (13b)$$

$$K = \begin{bmatrix} K_n & 0 \\ -\phi_n(a)k_T & k_T \end{bmatrix} \quad (13c)$$

$$Y = [u_n(x, t) \quad y_T(x, t)]^T \quad (13d)$$

$$F = [\phi_n(h)F(x, t) \quad 0]^T \quad (13e)$$

$$M_n = \bar{m}(x) \int_0^L [\phi_n(x)]^2 dx \quad (13f)$$

$$C_n = \bar{c}(x) \int_0^L [\phi_n(x)]^2 dx \quad (13g)$$

$$K_n = \left[EI \left(\frac{n\pi}{L} \right)^4 + T \left(\frac{n\pi}{L} \right)^2 \right] \int_0^L [\phi_n(x)]^2 dx \quad (13h)$$

where M_n, C_n, K_n denote the generalized mass matrix, generalized damping matrix, and generalized stiffness matrix for the n th order modal of the transmission line.

2.2. Displacement Response Spectrum

The displacement response spectrum is employed to analyze the vibration reduction effect of the TMDI for the transmission line. The closed-form solution of the displacement response spectrum of the transmission line with the ungrounded TMDI can be obtained in the Fourier domain as follows [35,38,41]:

$$Y(\omega) = H(\omega) \times F^*(\omega) \quad (14)$$

where $H(\omega)$ is the transfer function, which can be calculated as

$$H(\omega) = \left(-\omega^2 M + i\omega C + K \right)^{-1}. \quad (15)$$

The generalized load spectrum matrix is obtained as

$$F^*(\omega) = [\phi_n(h)F_n^*(\omega) \quad 0]^T. \quad (16)$$

The duration of the harmonic excitation is assumed as t_1 , the generalized load can be calculated as [42]

$$F_n^*(\omega) = \hat{f}(x) \frac{\bar{\omega}_n}{\omega^2 - \bar{\omega}_n^2} \left[\frac{(\omega + \bar{\omega}_n)}{2\bar{\omega}_n} e^{-i(\omega - \bar{\omega}_n)t_1} - \frac{(\omega - \bar{\omega}_n)}{2\bar{\omega}_n} e^{-i(\omega + \bar{\omega}_n)t_1} - 1 \right] \quad (17)$$

where $i = \sqrt{-1}$. The displacement response spectrum of the system is developed as

$$\mathbf{Y}(\omega) = \begin{Bmatrix} U_n(\omega) \\ Y_T(\omega) \end{Bmatrix} = \mathbf{A}^{-1} \mathbf{F}^*(\omega) \quad (18)$$

$$\mathbf{A} = \begin{bmatrix} A_1 & A_2 \\ A_3 & A_4 \end{bmatrix} \quad (19)$$

$$A_1 = -\omega^2 [M_n - \phi_n(a)\phi_n(d)b + \phi_n^2(d)b] + i\omega C_n + K_n \quad (20a)$$

$$A_2 = -\omega^2 [\phi_n(a)(m_T + b) - \phi_n(d)b] \quad (20b)$$

$$A_3 = \omega^2 \phi_n(d)b - i\omega \phi_n(a)c_T - \phi_n(a)k_T \quad (20c)$$

$$A_4 = -\omega^2(m_T + b) + i\omega c_T + k_T. \quad (20d)$$

Substituting Equation (19) into Equation (18), $U_n(\omega)$ is expressed as

$$U_n(\omega) = \frac{(-\omega^2(m_2 + b) + i\omega c_T + k_T) F_n^*(\omega)}{A_1 A_4 - A_2 A_3} \quad (21)$$

and the closed-form solution of the displacement response spectrum can be obtained as

$$y_n(\omega) = \phi_n(x) U_n(\omega). \quad (22)$$

Define the following parameters:

$$\omega_n = \sqrt{K_n/M_n}; \quad \omega_T = \sqrt{k_T/(m_T + b)} \quad (23a)$$

$$\mu = m_T/M_n; \quad \beta = b/m_T; \quad \gamma = \omega_T/\omega_n \quad (23b)$$

$$\zeta_T = c_T/2(m_T + b)\omega_T; \quad \zeta_n = C_n/2(M_n + b)\omega_n \quad (23c)$$

in which, ω_n , ω_T are the n th modal frequency of the transmission line and the natural frequency of the TMDI; μ , β , γ are the mass ratio, apparent mass ratio, and frequency ratio, respectively. ζ_T , ζ_n are the damping ratio of the TMDI and the n th modal damping ratio of the transmission line, respectively.

The closed-form solution of the displacement response spectrum of the transmission line-TMDI system is obtained as follows:

$$y_n(\omega) = \frac{\phi_n(x) \left(-\omega^2 + 2i\omega\omega_n\zeta_T\gamma + (\omega_n\gamma)^2 \right) \left(\phi_n(h)\hat{f}(x) \frac{\bar{\omega}_n}{\omega^2 - \bar{\omega}_n^2} \left(\frac{(\omega + \bar{\omega}_n)}{2\bar{\omega}_n} e^{-i(\omega - \bar{\omega}_n)t_1} - \frac{(\omega - \bar{\omega}_n)}{2\bar{\omega}_n} e^{-i(\omega + \bar{\omega}_n)t_1} - 1 \right) \right)}{A_1 \left(-\omega^2 + 2i\omega\omega_n\zeta_T\gamma + (\omega_n\gamma)^2 \right) + \left(\omega^2\phi_n(d)b - 2i\omega\omega_n\zeta_T\gamma\phi_n(a) - \phi_n(a)(\omega_n\gamma)^2 \right) (M_n\mu(1 + \beta)\phi_n(a) - \phi_n(d)b)\omega^2} \quad (24)$$

3. Vibration Control Performance Evaluation

To study the effect of the connection location of the inerter on the vibration control performance of the system, the suspension location factor is defined in this section. Then, based on the fixed-point theory, the optimized closed-form solutions for the damping ratio and frequency ratio of the TMDI are derived, respectively.

3.1. Parameter Optimization of TMDI

In terms of Equation (24), the displacement response spectrum of the transmission line is affected by the damping ratio and frequency ratio of the TMDI. To mitigate the maximum

amplitude of the displacement response, the optimal design for the TMDI is conducted in this section by the fixed-point theory [37].

Define the parameter v as the suspension location factor, which is

$$v = \frac{\phi_n(d) - \phi_n(a)}{2} \tag{25}$$

where $\phi_n(d), \phi_n(a)$ are the n th modal coordinates at the suspension locations of the inerter and mass of the TMDI. When the n th resonance of the system occurs, the Equation (12) can be re-expressed as follows by substituting Equation (25) into Equation (12),

$$[M_n - \phi_n(a)(\phi_n(a)+2v)b + (\phi_n(a)+2v)^2b]\ddot{u}_n + [\phi_n(a)(m_T + b) - (\phi_n(a)+2v)b]\ddot{y}_T + C_n\dot{u}_n + K_nu_n = \phi_n(h)F(x, t) \tag{26a}$$

$$- b(\phi_n(a)+2v)\ddot{u}_n + (m_T + b)\ddot{y}_T - \phi_n(a)c_T\dot{u}_n + c_T\dot{y}_T - \phi_n(a)k_Tu_n + k_Ty_T = 0 \tag{26b}$$

where the overdot indicates differentiation with respect to time. Because the external excitation is a harmonic load, the responses also have the characteristics of harmonics, and $F(x, t), u_n(t)$ are expressed as

$$F(x, t) = \hat{f}(x)e^{i\omega t} \tag{27a}$$

$$u_n(t) = \hat{u}_ne^{i\omega t}; \dot{u}_n(t) = i\omega\hat{u}_ne^{i\omega t}; \ddot{u}_n(t) = -\omega^2\hat{u}_ne^{i\omega t} \tag{27b}$$

$$y_T(t) = \hat{y}_Te^{i\omega t}; \dot{y}_T(t) = i\omega\hat{y}_Te^{i\omega t}; \ddot{y}_T(t) = -\omega^2\hat{y}_Te^{i\omega t} \tag{27c}$$

in which, \hat{u}_n and \hat{y}_T are the complex amplitude. By substituting Equation (29) into Equation (28), the response amplitude is obtained as

$$\hat{u}_n = \frac{\phi_n(h)\hat{f}(x)(k_T - b\omega^2 - m_T\omega^2 + c_T\omega i)}{\sigma_1 + \sigma_2} \tag{28a}$$

where

$$\sigma_1 = \omega^2[(b + m_T)\phi_n(a) - b(2v + \phi_n(a))][-k_2\phi_n(a) - c_Ti\omega\phi_n(a) + b\omega^2(2v + \phi_n(a))] \tag{28b}$$

$$\sigma_2 = [k_T + c_Ti\omega - (b + m_T)\omega^2][K_n + C_ni\omega - \omega^2(M_n - b\phi_n(a) + (2v + \phi_n(a)) + b(2v + \phi_n(a))^2)]. \tag{28c}$$

The equivalent static displacement amplitude of the host structure is defined as

$$X_{st} = \frac{F_n}{K_n}. \tag{29}$$

The dynamic amplification factor (DAF) of host structure can be expressed as follows

$$\left| \frac{X_1}{X_{st}} \right| = \frac{K_n\sqrt{\alpha_1^2 + \alpha_2^2}}{\sqrt{\alpha_3^2 + \alpha_4^2}} \tag{30}$$

$$\alpha_1 = k_T - b\omega^2 - m_T\omega^2 \tag{31a}$$

$$\alpha_2 = c_T\omega \tag{31b}$$

$$\alpha_3 = K_nk_T - (bK_n + k_TM_n + K_nm_T + \phi_n^2(a)k_Tm_T + 4v^2bk_T)\omega^2 + (bM_n + M_nm_T + 4v^2bm_T + 4bvm_T\phi_n(a) + bm_T\phi_n^2(a))\omega^4 \tag{31c}$$

$$\alpha_4 = (c_TK_n)\omega - (c_TM_n + 4v^2bc_T + \phi_n^2(a)c_Tm_T)\omega^3. \tag{31d}$$

In terms of the fixed-point theory, the curve of the DAF always passes through two fixed points (P and Q) in the frequency domain. Considering the transmission line structure

is a small damping structure, the host structure damping is assumed to be zero, which has been proved to be appropriate in the previous studies [43]. Hence, Equation (32) can be re-expressed as follows:

$$\left| \frac{X_1}{X_{st}} \right| = \sqrt{\frac{\left(1 - \frac{\lambda^2}{\gamma^2}\right)^2 + \left(\frac{2}{\gamma}\right)^2 (\xi_T \lambda)^2}{\left(\frac{1 + \beta + \mu\beta(2v + \phi_n(a))^2}{(1 + \beta)\gamma^2}\right) \lambda^4 - \left(1 + \frac{1}{\gamma^2} + \phi_n^2(a)\mu + 4v^2\mu\beta\right) \lambda^2 + 1} + \left(\frac{2 - 2(1 + 4v^2\mu\beta + \phi_n^2(a)\mu)\lambda^2}{\gamma}\right)^2 (\xi_T \lambda)^2}} \quad (32)$$

in which, $\lambda = \omega/\omega_n$. The optimal frequency ratio (γ_{opt}) and damping ratio (ξ_{Topt}) are expressed as [43]

$$\gamma_{opt} = \frac{\sqrt{1 + (1 + \phi_n^2(a)\mu + 4\phi_n(a)v\mu + 4v^2\mu)}}{(1 + \phi_n^2(a)\mu + 4v^2\mu\beta)\sqrt{(1 + \beta)}} \quad (33)$$

$$\xi_{Topt} = \sqrt{\frac{\xi^2(\lambda_P) + \xi^2(\lambda_Q)}{2}} \quad (34)$$

in which, $\xi^2(\lambda)$ is calculated as follows

$$\xi^2(\lambda) = \frac{\kappa_1 + \sqrt{\kappa_1^2 - 4\kappa_2\kappa_3}}{2\kappa_2} \quad (35)$$

where κ_1 , κ_2 and κ_3 are defined as

$$\kappa_1 = (3\Delta_1^2 F^2 + \Delta_4^2 \Delta_3^2) \lambda^8 - (4\Delta_4 \Delta_3^2 + 4\Delta_1 \Delta_2 \Delta_6^2) \lambda^6 + (\Delta_2^2 \Delta_6^2 + 4\Delta_4 \Delta_3 \Delta_5 + 3\Delta_3^2 + 2\Delta_1 \Delta_6^2 - \Delta_4^2 \Delta_5^2) \lambda^4 - (4\Delta_3 \Delta_5) \lambda^2 + (\Delta_5^2 - \Delta_6^2) \quad (36a)$$

$$\kappa_2 = -2\Delta_3^2 \Delta_6^2 \lambda^6 + 2\Delta_3 \Delta_5 \Delta_6^2 \lambda^4 \quad (36b)$$

$$\kappa_3 = (-2\Delta_1^2 \Delta_4^2) \lambda^{10} + (2\Delta_1 \Delta_2 \Delta_4^2 + 6\Delta_1^2 \Delta_4) \lambda^8 - (4\Delta_1^2 + 8\Delta_1 \Delta_2 \Delta_4) \lambda^6 + (6\Delta_1 \Delta_2 + 4\Delta_1 \Delta_4 + 2\Delta_2^2 \Delta_4 - 2\Delta_2 \Delta_4^2) \lambda^4 - (4\Delta_1 + 2\Delta_2^2 - 2\Delta_4^2) \lambda^2 - (2\Delta_2 - 2\Delta_4) \quad (36c)$$

in which, $\Delta_1 \sim \Delta_6$ are defined as

$$\Delta_1 = \frac{1 + \beta + \mu\beta(2v + \phi_n(a))^2}{(1 + \beta)\gamma^2} \quad (37a)$$

$$\Delta_2 = 1 + \frac{1}{\gamma^2} + \phi_n^2(a)\mu + 4v^2\mu\beta \quad (37b)$$

$$\Delta_3 = \frac{2(1 + 4v^2\mu\beta + \phi_n^2(a)\mu)}{\gamma} \quad (37c)$$

$$\Delta_4 = \frac{1}{\gamma^2}, \Delta_5 = \frac{2}{\gamma}, \Delta_6 = \frac{2}{\gamma} \quad (37d)$$

3.2. Vibration Control Performance Evaluation of TMDI

It can be observed that the connection location of the inerter has a significant effect on the vibration performance of the system. Therefore, it is necessary to discuss the optimal suspension location of the inerter for the system.

As can be seen from Figure 5a–f, when the mass ratio ($\mu = m_T/M_n$) is equal to 0.01, the variation of the suspension location factor (v) almost does not affect the optimal frequency ratio (γ_{opt}), the value of which is approximately equal to 0.96–0.98. When the mass ratio and the apparent mass ratio ($\beta = b/m_T$) are relatively large, i.e., $\mu = 0.06$ and $\beta = 0.6$, γ_{opt}

decreases by 13% with the increase of v from 0 to 1 and shows a slight nonlinearity. It is worth noting that when v is approximately equal to 0.2, γ_{opt} is not affected by μ and β . The inertial mass failure phenomenon has occurred.

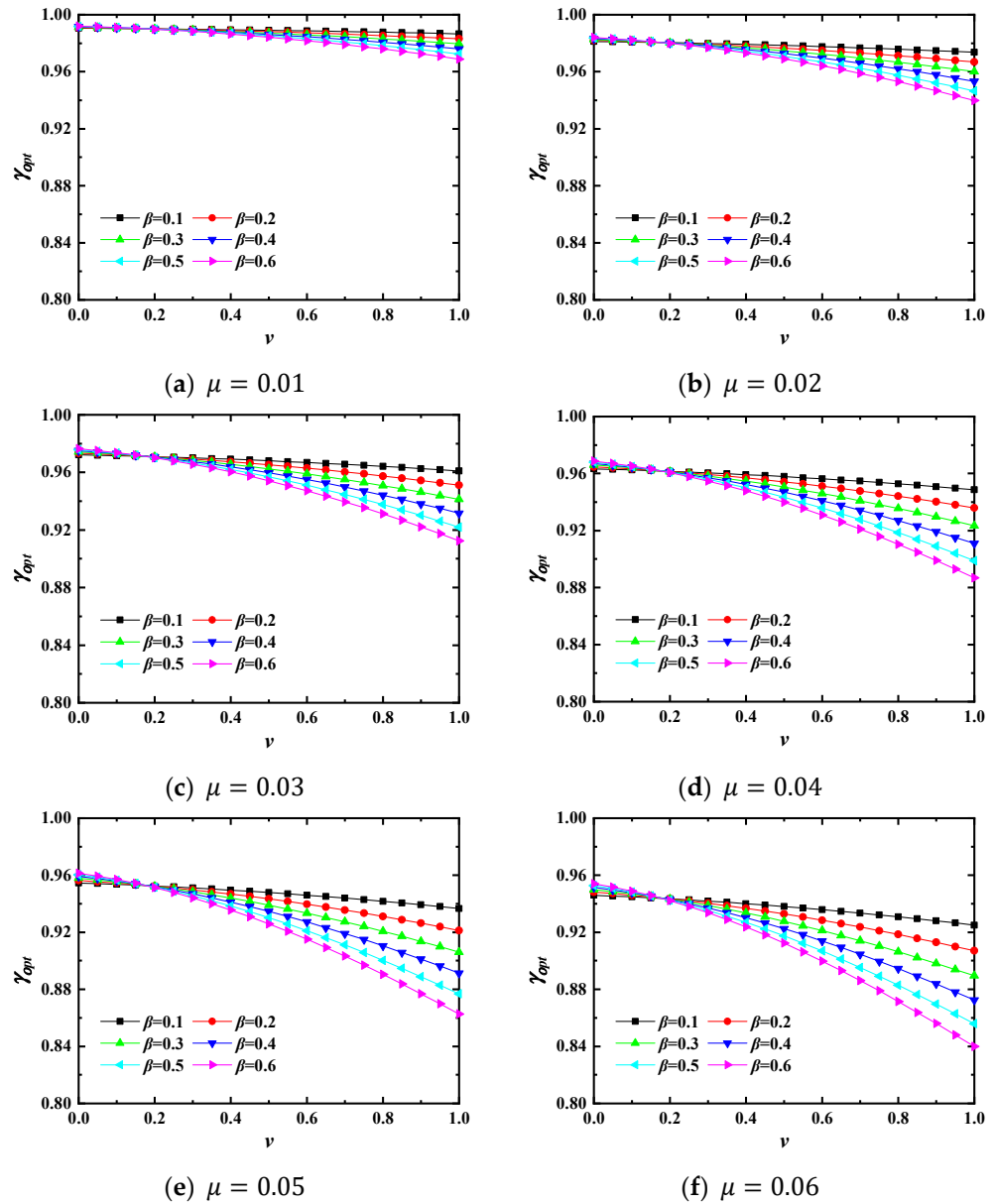


Figure 5. Optimal frequency ratio versus suspension location factor with different mass ratios and apparent mass ratios.

The optimal damping ratio (ζ_{opt}) increases linearly with the increase of v , as shown in Figure 6. When $\mu = 0.01$ and $\beta = 0.1$, the optimal frequency ratio increased by nearly 3% with the increase of v from 0 to 1. However, ζ_{opt} increases by 90% as v changes from 0 to 1 when μ and β increase to 0.06 and 0.6, respectively. And there is still a failure phenomenon of the inerter for ζ_{opt} when v is approximately equal to 0.23. In addition, the effect of β on the optimal damping ratio and the optimal frequency ratio is more significant than the effect of μ on them.

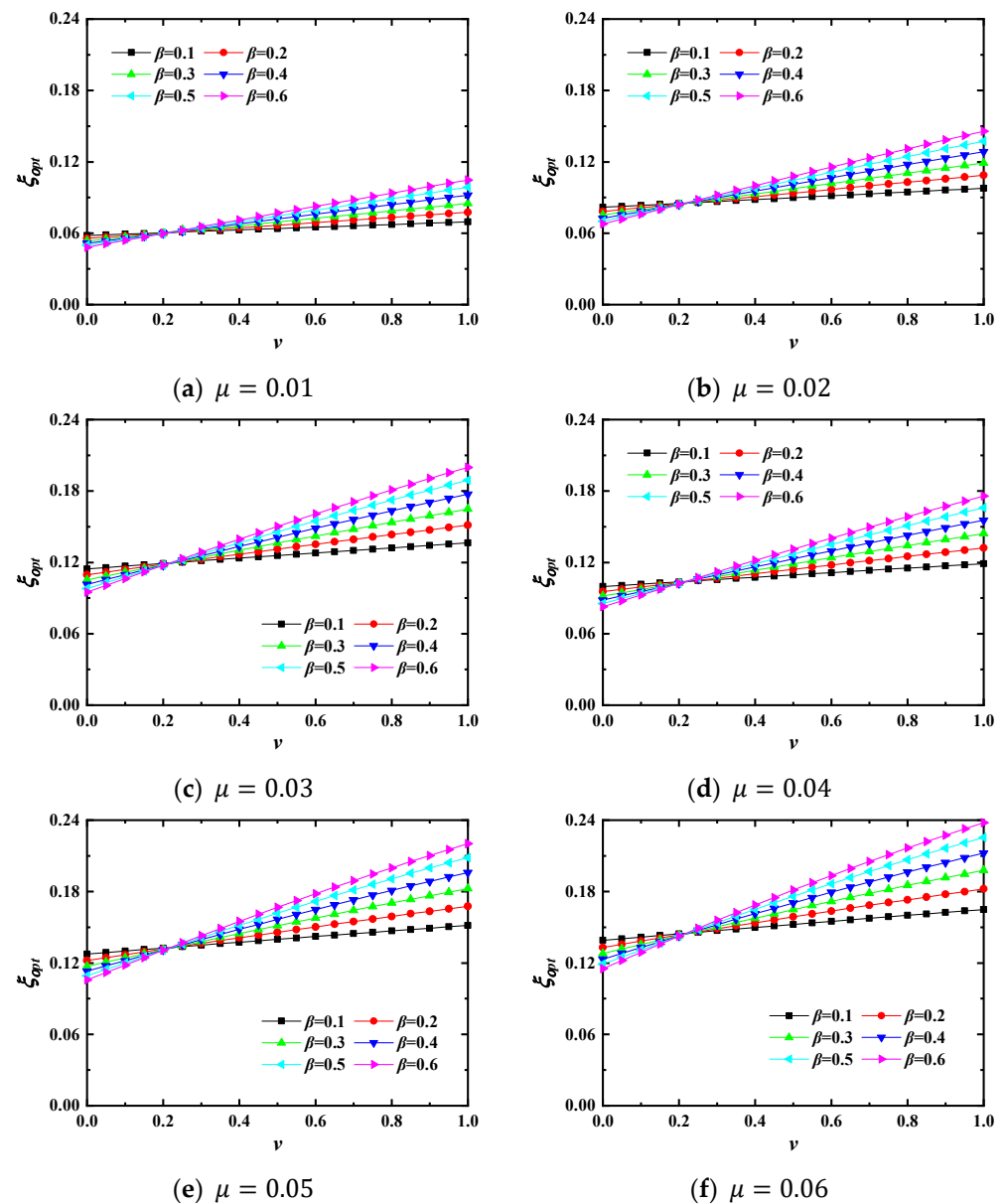


Figure 6. Optimal damping ratio versus suspension location factor with different mass ratios and apparent mass ratios.

For the peak value of the displacement response spectrum ($y(\omega)_{max}$), under the conditions that the mass ratio and the apparent mass ratio are relatively small, as shown in Figure 7a, the $y(\omega)_{max}$ shows a slight linear decreasing trend with the increase of ν . However, $y(\omega)_{max}$ decreases by about 30% with the range $0 < \nu < 1$, as μ and β increase up to 0.06 and 0.6, respectively. This indicates that the vibration suppression performance of the structure is significantly affected by the suspension location of the inerter.

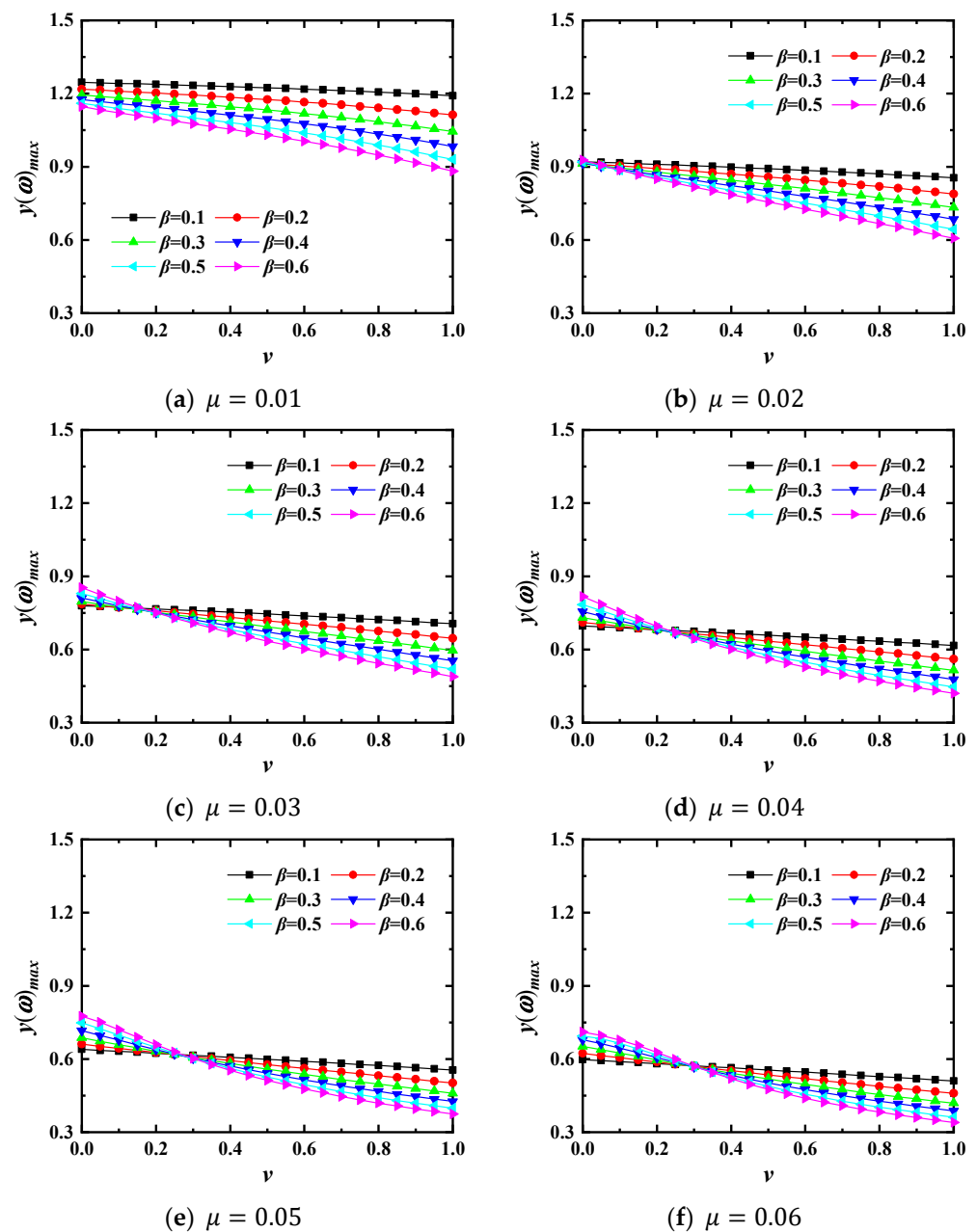


Figure 7. The peak value of displacement response versus suspension location factor with different mass ratios and apparent mass ratios.

As shown in Figure 7c–f, in the range of $v < 0.2$, the TMDI plays a negative role in vibration suppression. That means the distance between the connection location of the inerter and the mass of the TMDI should not be too small; otherwise, it will be detrimental to the vibration suppression of the ungrounded TMDI. When $v > 0.2$, the TMDI has a positive effect on the vibration suppression performance of the system. It is known that the ungrounded TMDI has the best effect on system vibration suppression when $v = 1.0$. With v approximately equal to 0.25, the failure phenomenon of the inerter is also observed for the peak displacement response spectrum, which should be avoided as much as possible in the design process of the vibration mitigation for transmission lines.

3.3. Discussion

In this section, a detailed discussion about the effectiveness of vibration control performance of TMDI used in transmission lines is carried out. By the fixed point theory,

the parameter optimization process of TMDI equipped with the transmission lines was developed. Through defining the suspension location factor, the effect of the location of the inerter on the optimal tuning frequency ratio (γ_{opt}) and the optimal tuning damping ratio (ζ_{opt}) was investigated. Figure 5 shows that γ_{opt} and ζ_{opt} decreases with the increase of v . However, for the optimal damping ratio, this trend is reversed, as shown in Figure 6. As the mass ratio (μ) and apparent mass ratio (β) increase, γ_{opt} and ζ_{opt} show a relatively strong nonlinear variation trend by the location of the inerter. The nonlinear influence of the apparent mass ratio on the optimized parameters is particularly significant. As shown in Figure 7, the vibration control performance of the transmission lines with an ungrounded TMDI is significantly influenced by the location of the inerter, which indicated that the suppression performance is significantly improved as the suspension location factor increases, especially at relatively high apparent mass ratios and mass ratios. However, it is important to note that there is a specific location ($v = 0.25\text{--}0.3$) to which the inertial mass should try to avoid being connected. Because the arrangement of the inertial mass in this area has minimal effect on the vibration suppression performance of the structure, which is incapable of demonstrating the vibration suppression benefits of the inerter-based vibration absorber.

4. Conclusions

In this paper, a novel ungrounded TMDI is proposed for the vibration control of a transmission line under harmonic excitation. The dynamic equations of the transmission line equipped with an ungrounded TMDI are derived. The closed-form solution of the displacement response spectrum is obtained in the Fourier domain. By the fixed-point theory, the optimal damping ratio, and the frequency ratio of the TMDI are derived, respectively. Finally, a detailed analysis of the vibration control performance of the inerter-based damper based on the suspension location of the inerter is carried out, and the main conclusions are obtained as follows.

(1) When the mass ratio is relatively small ($\mu = 0.01$), μ and β have a very limited effect on γ_{opt} . With the increase of the mass ratio (μ) and apparent mass ratio (β), γ_{opt} decreases with the increasing v , and exhibits a nonlinear trend. When $\mu = 0.06$ and $\beta = 0.6$, γ_{opt} decreases by nearly 13% as v increases from 0 to 1. The optimal damping ratio (ζ_{opt}) increases linearly with increasing v . When $\mu = 0.06$, $\beta = 0.6$, ζ_{opt} increases sharply by about 90% in the range of $0 < v < 1$.

(2) The suspension location factor (v) has a significant impact on the vibration reduction of the structure. In particular, when the mass ratio and apparent mass ratio are equal to 0.06 and 0.6, the peak of the displacement response spectrum decreases by about 30% as v increases from 0 to 1. When $\mu > 0.3$, $v < 0.25$, the inerter plays a negative role in the vibration control performance, which is due to the negative stiffness term in the dynamic equation.

(3) With the change of the suspension location of the inerter, the failure phenomenon of the inerter occurs, which is caused by a similar phase of the vibration response. The peak of the displacement response spectrum decreases linearly as v increases from 0 to 1. The transmission line equipped with the ungrounded TMDI has the best vibration suppression performance as v is equal to 1.

Author Contributions: Conceptualization, Y.Z. and Y.S.; methodology, Y.Y.; software, L.Z.; data curation, Y.Y.; writing—review and editing, X.L. All authors have read and agreed to the published version of the manuscript.

Funding: This research was funded by National Natural Science Foundation of China grant number 52008070.

Conflicts of Interest: The authors declare no conflict of interest.

References

1. Gabbai, R.; Benaroya, H. An overview of modeling and experiments of vortex-induced vibration of circular cylinders. *J. Sound Vib.* **2005**, *282*, 575–616. [[CrossRef](#)]
2. Williamson, C.; Govardhan, R. A brief review of recent results in vortex-induced vibrations. *J. Wind Eng. Ind. Aerodyn.* **2008**, *96*, 713–735. [[CrossRef](#)]
3. Wu, X.; Ge, F.; Hong, Y. A review of recent studies on vortex-induced vibrations of long slender cylinders. *J. Fluids Struct.* **2012**, *28*, 292–308. [[CrossRef](#)]
4. Mannini, C.; Marra, A.; Bartoli, G. VIV-galloping instability of rectangular cylinders: Review and new experiments. *J. Wind Eng. Ind. Aerodyn.* **2014**, *132*, 109–124. [[CrossRef](#)]
5. Chen, Z.; Tse, K.T.; Kwok, K.C.S.; Kareem, A.; Kim, B. Measurement of unsteady aerodynamic force on a galloping prism in a turbulent flow: A hybrid aeroelastic-pressure balance. *J. Fluids Struct.* **2021**, *102*, 103232. [[CrossRef](#)]
6. Zhou, L.; Yan, B.; Zhang, L.; Zhou, S. Study on galloping behavior of iced eight bundle conductor transmission lines. *J. Sound Vib.* **2016**, *362*, 85–110. [[CrossRef](#)]
7. Diana, G.; Belloli, M.; Giappino, S.; Manenti, A.; Mazzola, L.; Muggiasca, S.; Zuin, A. Wind Tunnel Tests on Two Cylinders to Measure Subspan Oscillation Aerodynamic Forces. *IEEE Trans. Power Deliv.* **2014**, *29*, 1273–1283. [[CrossRef](#)]
8. Diana, G.; Belloli, M.; Giappino, S.; Manenti, A.; Mazzola, L.; Muggiasca, S.; Zuin, A. A Numerical Approach to Reproduce Subspan Oscillations and Comparison with Experimental Data. *IEEE Trans. Power Deliv.* **2014**, *29*, 1311–1317. [[CrossRef](#)]
9. Hori, Y.; Okuyama, K. Axial Vibration Analysis of Transformer Windings Under Short Circuit Conditions. *IEEE Trans. Power Appar. Syst.* **1980**, PAS-99, 443–451. [[CrossRef](#)]
10. Bungay, E.; Mcallister, D. *Electric Cables Handbook*; CRC Press: Boca Raton, FL, USA, 1990.
11. Zhang, M.; Song, Y.; Abdelkefi, A.; Yu, H.; Wang, J. Vortex-induced vibration of a circular cylinder with nonlinear stiffness: Prediction using forced vibration data. *Nonlinear Dyn.* **2022**, *108*, 1867–1884. [[CrossRef](#)]
12. Liu, G.; Li, H.; Qiu, Z.; Leng, D.; Li, Z.; Li, W. A mini review of recent progress on vortex-induced vibrations of marine risers. *Ocean Eng.* **2020**, *195*, 106704. [[CrossRef](#)]
13. Jafari, M.; Hou, F.; Abdelkefi, A. Wind-induced vibration of structural cables. *Nonlinear Dyn.* **2020**, *100*, 351–421. [[CrossRef](#)]
14. Xu, F.; Yu, H. Effect of Ice Accretion on the Aerodynamic Responses of a Pipeline Suspension Bridge. *J. Bridg. Eng.* **2020**, *25*, 04020091. [[CrossRef](#)]
15. Weaver, D.; Fitzpatrick, J. A review of cross-flow induced vibrations in heat exchanger tube arrays. *J. Fluids Struct.* **1988**, *2*, 73–93. [[CrossRef](#)]
16. Zhang, M.; Xu, F. Tuned mass damper for self-excited vibration control: Optimization involving nonlinear aeroelastic effect. *J. Wind. Eng. Ind. Aerodyn.* **2022**, *220*, 104836. [[CrossRef](#)]
17. Zucca, M.; Longarini, N.; Simoncelli, M.; Aly, A.M. Tuned Mass Damper Design for Slender Masonry Structures: A Framework for Linear and Nonlinear Analysis. *Appl. Sci.* **2021**, *11*, 3425. [[CrossRef](#)]
18. Stockbridge, G.H. Vibration Damper. U.S. Patent 1,675,391, 3 July 1928.
19. Claren, R.; Diana, G. Mathematical analysis of transmission line vibration. *IEEE Trans. Power Appar. Syst.* **1969**, PAS-88, 1741–1771. [[CrossRef](#)]
20. Wagner, H.; Ramamurti, V.; Sastry, R.; Hartmann, K. Dynamics of Stockbridge dampers. *J. Sound Vib.* **1973**, *30*, 207–220. [[CrossRef](#)]
21. Leblond, A.; Hardy, C. On the estimation of a 2×2 complex stiffness matrix of symmetric Stockbridge-type dampers. In Proceedings of the 3rd International Symposium on Cable Dynamics, Trondheim, Norway, 10 August 1999.
22. Luo, X.; Wang, L.; Zhang, Y. Nonlinear numerical model with contact for Stockbridge vibration damper and experimental validation. *J. Vib. Control* **2014**, *22*, 1217–1227. [[CrossRef](#)]
23. Vaja, N.K.; Barry, O.; DeJong, B. Finite element modeling of Stockbridge damper and vibration analysis: Equivalent cable stiffness. In Proceedings of the International Design Engineering Technical Conferences and Computers and Information in Engineering Conference—ASME, Cleveland, OH, USA, 6–9 August 2017. [[CrossRef](#)]
24. Richardson, A.S. Vibration damping required for overhead lines. *IEEE Trans. Power Deliv.* **1995**, *10*, 934–940. [[CrossRef](#)]
25. Vecchiarelli, J.; Currie, I.; Havard, D. Computational analysis of aeolian conductor vibration with a Stockbridge-type damper. *J. Fluids Struct.* **2000**, *14*, 489–509. [[CrossRef](#)]
26. Zhang, B.; Gong, W.S.; Wang, Z.H.; Zhang, M.G.; Han, L.; Zhang, Y. Study on equivalent viscous damping of aeolian vibration for transmission line by AACSR-400 steel core aluminum alloy wire. *Key Eng. Mater.* **2016**, *723*, 94–99. [[CrossRef](#)]
27. Smith, M. Synthesis of mechanical networks: The inerter. *IEEE Trans. Autom. Control* **2002**, *47*, 1648–1662. [[CrossRef](#)]
28. Marian, L.; Giaralis, A. Optimal design of a novel tuned mass-damper-inerter (TMDI) passive vibration control configuration for stochastically support-excited structural systems. *Probabilistic Eng. Mech.* **2014**, *38*, 156–164. [[CrossRef](#)]
29. Pan, C.; Zhang, R. Design of structure with inerter system based on stochastic response mitigation ratio. *Struct. Control Heal. Monit.* **2018**, *25*, e2169. [[CrossRef](#)]
30. Giaralis, A.; Petrini, F. Wind-Induced Vibration Mitigation in Tall Buildings Using the Tuned Mass-Damper-Inerter. *J. Struct. Eng.* **2017**, *143*, 04017127. [[CrossRef](#)]
31. Petrini, F.; Giaralis, A.; Wang, Z. Optimal tuned mass-damper-inerter (TMDI) design in wind-excited tall buildings for occupants' comfort serviceability performance and energy harvesting. *Eng. Struct.* **2020**, *204*, 109904. [[CrossRef](#)]

32. Wang, Q.; Qiao, H.; De Domenico, D.; Zhu, Z.; Xie, Z. Wind-Induced Response Control of High-Rise Buildings Using Inerter-Based Vibration Absorbers. *Appl. Sci.* **2019**, *9*, 5045. [[CrossRef](#)]
33. Su, N.; Xia, Y.; Peng, S. Filter-based inerter location dependence analysis approach of Tuned mass damper inerter (TMDI) and optimal design. *Eng. Struct.* **2022**, *250*, 113459. [[CrossRef](#)]
34. Dai, J.; Xu, Z.-D.; Gai, P.-P. Tuned mass-damper-inerter control of wind-induced vibration of flexible structures based on inerter location. *Eng. Struct.* **2019**, *199*, 109585. [[CrossRef](#)]
35. Zhang, Z.; Fitzgerald, B. Tuned mass-damper-inerter (TMDI) for suppressing edgewise vibrations of wind turbine blades. *Eng. Struct.* **2020**, *221*, 110928. [[CrossRef](#)]
36. De Domenico, D.; Ricciardi, G. An enhanced base isolation system equipped with optimal tuned mass damper inerter (TMDI). *Earthq. Eng. Struct. Dyn.* **2018**, *47*, 1169–1192. [[CrossRef](#)]
37. Den Hartog, J.P. *Mechanical Vibrations*; Courier Corporation: Chelmsford, MA, USA, 1985.
38. Wang, Z.; Giaralis, A. Enhanced motion control performance of the tuned mass damper inerter (TMDI) through primary structure shaping. *Struct. Control Heal. Monit.* **2021**, *28*, e2756. [[CrossRef](#)]
39. Kaveh, A.; Mahdavi, V. Colliding bodies optimization: A novel meta-heuristic method. *Comput. Struct.* **2014**, *139*, 18–27. [[CrossRef](#)]
40. Kaveh, A.; Farzam, M.F.; Jalali, H.H.; Maroofiazar, R. Robust optimum design of a tuned mass damper inerter. *Acta Mech.* **2020**, *231*, 3871–3896. [[CrossRef](#)]
41. Zhou, S.; Jean-Mistral, C.; Chesne, S. Influence of inerters on the vibration control effect of series double tuned mass dampers: Two layouts and analytical study. *Struct. Control Health Monit.* **2019**, *26*, e2414. [[CrossRef](#)]
42. Li, J.; Zhang, H.; Chen, S.; Zhu, D. Optimization and sensitivity of TMD parameters for mitigating bridge maximum vibration response under moving forces. *Structures* **2020**, *28*, 512–520. [[CrossRef](#)]
43. Wang, Z.; Li, H.-N.; Song, G. Aeolian vibration control of power transmission line using Stockbridge type dampers—A review. *Int. J. Struct. Stab. Dyn.* **2021**, *21*, 2130001. [[CrossRef](#)]